Available online at www.sciencedirect.com
ScienceDirect
Journal of Catalysis 252 (2007) 49–56
JOURNAL OF CATALYSIS
www.elsevier.com/locate/jcat

Dimethyl ether combustion catalyzed by supported Pd, Rh, and Pt clusters: Site requirements and reaction pathways

Akio Ishikawa, Enrique Iglesia *

Department of Chemical Engineering, University of California, Berkeley, CA 94720, USA

Received 13 June 2007; revised 27 August 2007; accepted 28 August 2007

Abstract

Clusters of Pt and Pd catalyze dimethyl ether (DME) combustion to CO_2 and H_2O at 400–600 K without detectable formation of byproducts. Rh clusters are less active and also form CO, HCHO, and CH_3OH in this temperature range. On Pd, isotopic and kinetic studies have shown that DME–O_2 reactions proceed via redox cycles limited by hydrogen abstraction from chemisorbed DME molecules without the involvement of methoxide intermediates in kinetically relevant steps, as shown previously on Pt clusters. Kinetic inhibition by H_2O is much stronger on Pd than on Pt clusters, apparently because of weaker binding of chemisorbed oxygen (O*) and hydroxyl (OH*) groups on Pt than on Pd. H_2O titrates vacancies (*) required to chemisorb DME molecules involved in kinetically relevant H-abstraction steps. DME combustion turnover rates (per exposed metal atom) on Pt, Pd, and Rh increased with increasing cluster size, but were not affected by the identity of the support (Al_2O_3, ZrO_2). These size effects reflect the stronger binding of O* and OH* on smaller clusters, which contain surface atoms with fewer neighbors and greater coordinative unsaturation. The higher reactivity of Pt compared with Pd and Rh also reflects the weaker binding of O* on Pt surfaces and the higher density of vacancies and of DME intermediates interacting with such vacancies. These trends resemble those reported for CH_4–O_2 on Pt and Pd clusters. They represent a general feature of reactions that require vacancies and the abstraction of H-atoms by basic oxygens on surfaces covered predominately by O* or OH* during catalysis.

Keywords: Dimethyl ether combustion; Supported metal clusters; Kinetic isotope effects; Cluster size and metal dispersion effects

1. Introduction

Dimethyl ether (DME; CH_3OCH_3) can be produced from C_1 feedstocks by one-step processes and is emerging as a replacement for liquefied petroleum gas (LPG) and diesel fuel in developing countries [1,2]. Several studies have described homogeneous DME pyrolysis and oxidation pathways that proceed via free-radical chain cycles [3–7]. These homogeneous reactions become detectable at 500–600 K and form predominately CO, CH_4, HCHO, and HCOOH at these low temperatures, with CO_2 and H_2O forming exclusively above 1000 K [8]. Catalytic routes decrease the temperature required for complete oxidation [9,10] and minimize NO_x and CO emissions ubiquitous in homogeneous reactions, making it possible to use DME as a clean fuel in power generation, food preparation, and space heating applications. Catalytic DME combustion on Pt clusters forms H_2O and CO_2 as the only detectable products at much lower temperatures (∼423 K) than homogeneous combustion (>1000 K); homogeneous pathways also form NO_x at the higher temperatures required for complete combustion [8].

We have recently described the details of DME combustion pathways on supported Pt clusters [8]. DME combustion turnover rates are limited by C–H bond activation in chemisorbed DME, a step that forms methoxy methyl intermediates, on site pairs consisting of chemisorbed oxygen atoms (O*) with vicinal vacancy sites (*) present on surfaces nearly saturated with O* [8]. DME turnover rates depend on reactant (DME, O_2) and product (CO_2, H_2O) concentrations, as well as on Pt cluster size, because such factors determine the density of (O*)–(*) site pairs required to abstract H atoms from adsorbed DME molecules in kinetically relevant steps. Acidic supports, such as γ-Al_2O_3, lead to bifunctional pathways involving DME reactions with H_2O formed in combustion steps

* Corresponding author.
E-mail address: iglesia@berkeley.edu (E. Iglesia).

0021-9517/$ – see front matter
doi:10.1016/j.jcat.2007.08.012

Table 1
Treatment conditions, metal dispersion, average crystallite diameter, and DME turnover rates (1% DME conversion)[a]

Catalyst	Treatment		Metal dispersion	Crystallite diameter (nm)[b]	DME turnover rate[c]
	Dry air	H_2			
0.8 wt% Pt/Al_2O_3	823 K, 5 h	723 K, 2 h	0.99	1.2	0.10
0.9 wt% Pt/Al_2O_3	823 K, 5 h	723 K, 2 h	0.75	1.6	0.19
0.9 wt% Pt/Al_2O_3	823 K, 5 h	873 K, 2 h	0.52	2.2	0.33
1.0 wt% Pt/ZrO_2	823 K, 5 h	823 K, 2 h	0.42	2.7	0.51
1.0 wt% Pt/ZrO_2	823 K, 5 h	873 K, 2 h	0.36	3.2	0.56
1.1 wt% Pt/ZrO_2	823 K, 5 h	873 K, 2 h	0.44	2.5	0.31
0.4 wt% Pd/Al_2O_3	823 K, 5 h	773 K, 2 h	0.51	2.2	0.10
0.7 wt% Pd/Al_2O_3	823 K, 5 h	773 K, 2 h	0.39	2.9	0.11
0.7 wt% Pd/Al_2O_3	823 K, 5 h	973 K, 2 h	0.23	4.9	0.15
0.9 wt% Pd/ZrO_2	823 K, 5 h	773 K, 2 h	0.17	6.5	0.15
0.9 wt% Rh/Al_2O_3	873 K, 5 h	873 K, 2 h	0.81	1.3	0.01
0.9 wt% Rh/Al_2O_3	1023 K, 5 h	873 K, 2 h	0.42	2.6	0.02
0.9 wt% Rh/Al_2O_3	1123 K, 5 h	873 K, 2 h	0.12	9.1	0.08

[a] 473 K, 2 kPa DME, 20 kPa O_2, balance He.
[b] Estimated from fractional metal dispersion assuming hemispherical clusters.
[c] Moles DME/g atom surface metal s (1% DME conversion).

to form CH_3OH, which reacts with O_2 much faster than DME on Pt clusters [11].

The identity and size of metal clusters strongly influence the rates and selectivities of catalytic reactions [12–17]. Specifically, reactions of CH_4 with H_2O or CO_2 on metal clusters, also limited by C–H bond activation steps, occur with the highest turnover rates on Pd [12], whereas the reactivity of other noble metals decreases in the sequence Pt > Ir > Rh [13]. In contrast, Pt shows higher reactivity than Pd for combustion of higher hydrocarbons [14–17].

Here we report DME combustion rates on Pd, Rh, and Pt clusters on γ-Al_2O_3 and ZrO_2 supports with a range of metal dispersions (0.12–0.99) and cluster sizes (∼1–10 nm). DME combustion turnover rates increased with increasing cluster size on all catalysts. For a given metal dispersion, the turnover rates were highest on Pt clusters and lowest on Rh clusters. We also extend our previous mechanistic studies on Pt to Pd clusters by providing kinetic and isotopic evidence for the involvement of (O*)–(*) site pairs in kinetically relevant steps involving the activation of C–H bonds in molecularly adsorbed DME.

2. Experimental

ZrO_2 (34 $m^2\,g^{-1}$), γ-Al_2O_3 (193 $m^2\,g^{-1}$), and SiO_2 (280 $m^2\,g^{-1}$, diluent) were prepared as reported previously [8,18]. Metal clusters were deposited by incipient wetness impregnation of Al_2O_3 and ZrO_2 with an aqueous solution of the respective precursor salts [$H_2PtCl_6{\cdot}6H_2O$ (Aldrich, CAS 16941-12-1, 99%), $Pd(NO_3)_2$ (Aldrich; lot 380040, 99.999%), and $(NH_4)_3RhCl_6$ (Alfa, CAS 10294-41-4, 99.99%)]. Impregnated supports for Pt and Pd samples were treated in ambient air at 393 K and then in flowing dry air (Praxair, 99.99%, 0.7 $cm^3\,g^{-1}\,s^{-1}$) at 823 K (0.083 $K\,s^{-1}$) for 5 h. Pt samples were prepared as reported previously [8]. Supported Pd samples were then exposed to flowing H_2 (Praxair, 99.999%, 0.8 $cm^3\,g^{-1}\,s^{-1}$) at 773 K (0.083 $K\,s^{-1}$) for 1 h and finally to 1% O_2/He (Praxair, 0.4 $cm^3\,g^{-1}\,s^{-1}$) at ambient temperature for 1 h to passivate the samples before exposing them to ambient air and use in rate and chemisorption measurements. Some of these Pd samples were treated again in flowing H_2 at 973 K for 2 h and passivated in 1% O_2/He (Praxair, 0.4 $cm^3\,g^{-1}\,s^{-1}$) before being exposed to ambient air, to vary Pd dispersion and cluster size. Rh samples were treated in flowing dry air (0.7 $cm^3\,g^{-1}\,s^{-1}$) at 873 K for 5 h. Portions of the Rh/Al_2O_3 samples were then treated again in flowing dry air at the temperatures noted in Table 1, to vary their dispersion. These Rh samples were then exposed to flowing H_2 (0.8 $cm^3\,g^{-1}\,s^{-1}$) at 873 K for 2 h and to 1% O_2/He (0.4 $cm^3\,g^{-1}\,s^{-1}$) at ambient temperature for 1 h before being exposed to ambient air.

The Pt, Pd, and Rh contents were measured by inductively coupled plasma-optical emission spectroscopy (ICP-OES; Galbraith Laboratories). Rh dispersions were measured from volumetric H_2 chemisorption uptakes at 313 K using a Quantasorb chemisorption analyzer (Quantachrome Corp.). A H_2 adsorption isotherm was measured at 3–50 kPa H_2 after treatment in flowing H_2 at 523 K for 1 h and then in dynamic vacuum at 523 K for 1 h. A back-sorption isotherm was then measured after evacuation at 313 K for 0.5 h. The two isotherms were extrapolated to zero H_2 pressure, and their difference was used to determine Rh dispersion by assuming a 1:1 H:Rh surface stoichiometry. Pd dispersions were measured from volumetric O_2 chemisorption uptakes at 313 K after treatment in pure H_2 at 673 K for 1 h and evacuation at 673 K for 1 h, assuming a 1:1 O:Pd surface stoichiometry. Pt dispersion was measured from volumetric uptakes of strongly chemisorbed H_2 as described previously [8]. Average diameters were estimated for each sample from these dispersion values by assuming hemispherical clusters and bulk metal densities (Rh, 12.4 $g\,cm^{-3}$; Pd, 11.3 $g\,cm^{-3}$; Pt, 21.45 $g\,cm^{-3}$ [19]). The metal dispersions and average cluster diameters are reported in Table 1.

DME combustion turnover rates were measured on samples (Rh, 8 mg; Pd, 5–100 mg; Pt, 5 mg catalyst) diluted with SiO_2 within pellets to avoid temperature gradients. Reactant and product concentrations were measured by gas chromatography

(Agilent 6890, with flame ionization and thermal conductivity detectors) using a methyl silicone capillary column (HP-1, 25 m × 0.32 mm × 1.05 μm) and a Porapak Q packed column (80–100 mesh, 144 cm, 3.2 mm).

Kinetic isotope effects (CH_3OCH_3–CD_3OCD_3, H_2O–D_2O) were measured on 0.9 wt% Pd/ZrO_2 (0.17 dispersion) catalysts using a gradientless recirculating batch reactor within which reactants and products were circulated over catalyst samples (60–100 mg; diluted with SiO_2, 5:1) at 1.7 $cm^3\ s^{-1}$ using a graphite gear micropump. Chemical and isotopic compositions were measured using a gas chromatograph (Agilent 6890) equipped with mass selective and flame ionization detectors.

3. Results and discussion

3.1. Dimethyl ether combustion rates on supported Pd clusters

Pd, Rh, and Pt metal clusters chemisorb O_2 dissociatively at ambient temperature [8,20–22]. Pt clusters have been shown to be present as metals by X-ray absorption near-edge spectroscopy (XANES) during DME combustion at 473 K [8]. These conclusions are consistent with the reported bulk oxidation of Pt clusters to PtO_2 in O_2 at only above ∼750 K, because the formation of superficial oxide protects the bulk metal from further oxidation [8,23–25]. But Pd and Rh clusters easily form their respective bulk oxides at the temperature (473 K) used here for DME catalytic combustion in the presence of O_2 [20–22]. In contrast, the reductant provided by the co-reactant decreases oxygen chemical potentials at surfaces and typically prevents the formation of bulk oxides. Surface-enhanced Raman spectra during methanol oxidation on Pd and Rh ultrathin films (about three to five monolayers) on gold substrates [26–28] at conditions similar to those used here for DME catalytic combustion (<573 K, 3 kPa CH_3OH, 80 kPa O_2) have shown that the bulk of those thin films remains metallic during catalysis. Therefore, we assume that Pd and Rh clusters also remained metallic during DME oxidation.

Fig. 1 shows DME turnover rates as a function of residence time at 473 K on 0.9 wt% Pd/ZrO_2 (0.17 dispersion) catalysts with different intrapellet dilution ratios at pellet diameters ranging from 250 to 450 μm. Intrapellet dilution ratios (2:1–6:1) did not influence DME combustion rates, indicating that measured rates were not corrupted by intrapellet temperature or concentration gradients, ubiquitous in combustion catalysis. Much larger dilution ratios (50:1) were required for Pt-based catalysts, because of their higher reactivity in DME combustion reactions [8]. On Pt catalysts, the inhibition of combustion rates by H_2O was rigorously excluded from the reported turnover rates by measuring rates as a function of residence time and extrapolating these rates to zero conversion. H_2O inhibition effects on Pd-based catalysts were much stronger and detectable even at very low conversions (0.4–4.8%); as a result, they contributed to measured rates even after these rates were extrapolated to zero DME conversion. Strong inhibition by H_2O also was prevalent for CH_4 combustion on PdO_x/ZrO_2 catalysts, because of significant coverage by chemisorbed OH* intermediates formed via quasi-equilibrated dissociative chemisorption of H_2O by products of combustion reactions [22].

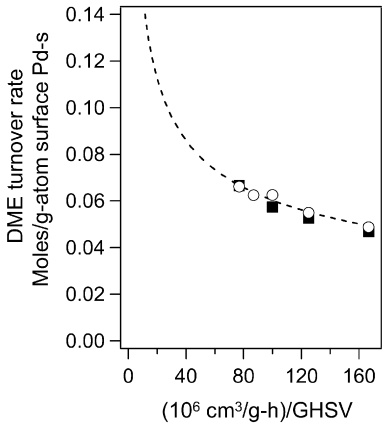

Fig. 1. DME combustion turnover rate as a function of residence time on 0.9 wt% Pd/ZrO_2 (60 mg, 0.17 dispersion) at 473 K for different SiO_2:catalyst intrapellet dilution ratios. 2 kPa DME, 20 kPa O_2, balance He; (○) 250–450 μm, 6:1; (■) 250–450 μm, 2:1; (dashed line) calculated DME turnover rates by interpolating average partial pressure of reactants and products using kinetic rate expressions obtained when OH* species are the most abundant surface intermediates.

$$CH_3OCH_3 + * \overset{K_1}{\rightleftharpoons} CH_3OCH_3\text{-}* \quad (1.1)$$

$$CH_3OCH_3\text{-}* + O* \overset{k_2}{\longrightarrow} CH_3OCH_2\text{-}* + OH* \quad (1.2)$$

$$\bullet\bullet\bullet\bullet\bullet$$

$$2OH* \overset{K_3}{\rightleftharpoons} H_2O + * + O* \quad (1.3)$$

$$CO_2* \overset{K_4}{\rightleftharpoons} CO_2 + * \quad (1.4)$$

$$O_2 + 2* \overset{k_5}{\longrightarrow} 2O* \quad (1.5)$$

Scheme 1. Reaction pathways for DME combustion on supported Pt and Pd clusters.

The effects of DME, O_2, and H_2O concentrations on DME turnover rates on Pd clusters are described by a rate equation (Eq. (4)) derived from the sequence of elementary steps shown in Scheme 1, with the assumptions that (OH*) species are the most abundant surface intermediates (MASI) and that their coverage is determined by quasi-equilibrated hydroxyl recombination steps. The dashed line in Fig. 1 reflects the effects of residence time on DME conversion predicted by this model as a result of the concurrent changes in the prevailing H_2O concentration with increasing DME conversion.

The kinetic response of DME combustion rates to DME and O_2 partial pressures was measured at 473 K on Pd/ZrO_2 (0.9 wt%, 0.17 dispersion) with added H_2O (5 kPa), so as to remove uncertainties introduced by water concentration gradients that otherwise would prevail along the catalyst bed. Fig. 2 shows the effects of DME and O_2 pressures on combustion turnover rates measured at low DME conversions (<1.5%) and constant flow rates (330 $cm^3\ g^{-1}\ s^{-1}$). For comparison, the figure also shows the kinetic response of DME combustion rates for 1.0 wt% Pt/ZrO_2 (0.42 dispersion). On both catalysts, DME turnover rates were proportional to DME concentrations and nearly independent of O_2 pressures, but this was the case for Pt-

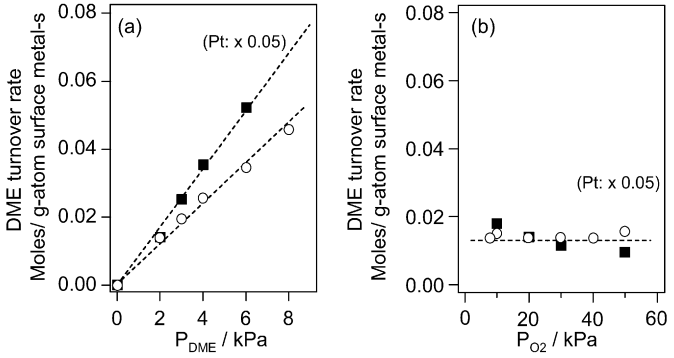

Fig. 2. Effects of DME (a) and O_2 (b) partial pressures on DME combustion turnover rates on 0.9 wt% Pd/ZrO_2 (○, 60 mg, 0.17 dispersion, 250–450 μm, 6:1 dilution with SiO_2) and 1.0 wt%. Pt/ZrO_2 (■, 5 mg, 0.42 dispersion, 250–450 μm, 50:1 dilution with SiO_2) with added H_2O (5 kPa) at 473 K. (20 kPa O_2 in (a) and 2 kPa DME in (b).)

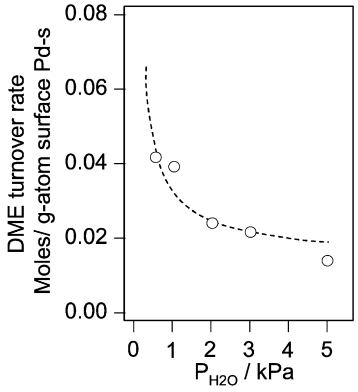

Fig. 3. Effect of H_2O partial pressures on DME combustion turnover rates on 0.9 wt% Pd/ZrO_2 at 473 K. (60 mg, 0.17 dispersion, 250–450 μm, 6:1, total flow rate 330 $cm^3\ g^{-1}\ s^{-1}$, 20 kPa DME, 20 kPa O_2, dashed curve: a regression of the data to the $1/H_2O$.)

based catalysts only when H_2O was present at significant concentrations due to its presence in the DME–O_2 reactant stream.

DME turnover rates decreased with increasing H_2O pressure on 0.9 wt% Pd/ZrO_2 (Fig. 3). A negative kinetic order in H_2O (-0.8 ± 0.2) was found by regressing the data (dashed curve) in Fig. 3 to a simple, albeit nonrigorous, power law kinetic equation. The dashed curves in Figs. 2 and 3 show that DME combustion turnover rates on Pd catalysts can be described accurately by

$$r = k(\mathrm{DME})^1(\mathrm{O_2})^0(\mathrm{H_2O})^{-1}. \quad (1)$$

This kinetic response to changes in DME, O_2, and H_2O concentrations was similar to that found for CH_4 combustion rates ($[CH_4]^1$, $[O_2]^0$, and $[H_2O]^{-1}$) on supported Pd clusters [22], suggesting a possible mechanistic resemblance in the combustion of these two reactants. In what follows, we describe a set of elementary steps consistent with this kinetic response.

3.2. Elementary steps involved in DME combustion reactions on Pd

The kinetic response of the DME combustion rate on Pd/ZrO_2 to DME and O_2 pressures was similar to that measured on Pt/ZrO_2 with H_2O present. These similarities suggest a mechanistic resemblance, but also a much stronger H_2O inhibition effect on Pd than on Pt clusters. The elementary steps are similar to those previously proposed for Pt-based catalysts (Scheme 1, [8]) consist of a catalytic sequence in which oxygen atoms in DME interact with vacancies on Pd surfaces (*) (step 1.1). Vicinal oxygen species (O*) then abstract H atoms from chemisorbed DME molecules in kinetically relevant steps without any intervening DME dissociation steps that would form methoxide species (step 1.2); these hydrogen abstraction steps are consistent with isotopic measurements and with density functional theory calculations on Pt catalysts [8]. The quasi-equilibrated desorption of OH* species from surfaces of Pd clusters to form water (step 1.3) and of chemisorbed CO_2 (step 1.4) then complete a catalytic cycle by forming vacancies (*) required for DME chemisorption; these vacancies are ultimately replaced by chemisorbed oxygen in irreversible step 1.5. In turn, the reversible dissociation and strong binding of water molecules as OH* cause the strong kinetic inhibition observed. A pseudo-steady-state treatment of the sequence in Scheme 1 leads to the rate equation (2). The terms in the denominator reflect the relative concentrations of the various adsorbed species [*, O*, adsorbed DME (DME*), OH*, and CO_2*]; derivation details have been given previously [8]. When O* species are the most abundant surface intermediates, this equation becomes

$$r = \frac{4.5(K_1k_2[\mathrm{DME}])^2}{k_5[\mathrm{O_2}]} \quad (3)$$

as found on Pt catalysts at low H_2O concentrations [8]. On the Pd catalysts, the turnover rates did not obey this kinetic dependence, even without added H_2O or at low DME conversions (<5%). The observed inhibition effects of water led us to consider OH* species as MASI, which led instead to a simplified version of Eq. (2),

$$r = \frac{K_1k_2K_3[\mathrm{DME}]}{[\mathrm{H_2O}]}. \quad (4)$$

$$r = \frac{k_5[\mathrm{O_2}]}{4.5 \times \left(1 + \left(\frac{k_5[\mathrm{O_2}]}{4.5K_1k_2[\mathrm{CH_3OCH_3}]}\right) + K_1[\mathrm{CH_3OCH_3}] + \left(\frac{k_5[\mathrm{H_2O}][\mathrm{O_2}]}{4.5K_1K_3k_2[\mathrm{CH_3OCH_3}]}\right)^{0.5} + \frac{[\mathrm{CO_2}]}{K_4}\right)^2}$$

* O* DME* OH* CO_2*

Equation 2.

Table 2
Kinetic isotope effects on 0.9 wt% Pd/ZrO_2 (2 kPa CH_3OCH_3 or CD_3OCD_3, 20 kPa O_2, 1 kPa H_2O or D_2O, 3 kPa Ar, 100 kPa total pressure, balance He, 1% DME conversion)

	Kinetic isotope effect (r_H/r_D)	
	473 K	503 K
CH_3OCH_3 + (H_2O vs D_2O)	1.0	1.0
CD_3OCD_3 + (H_2O vs D_2O)	1.0	1.1
(CH_3OCH_3 vs CD_3OCD_3) + H_2O	3.8	2.6
(CH_3OCH_3 vs CD_3OCD_3) + D_2O	3.9	2.9
(CH_3OCH_3 + H_2O vs CD_3OCD_3 + D_2O)	3.8	2.9

This equation accurately describes measured DME combustion rates $\{r \sim [\mathrm{DME}]^1[\mathrm{O_2}]^0; [\mathrm{H_2O}]^{-1}\}$ (Figs. 2 and 3; Eq. (1)). The DME turnover rates on Pt catalysts also exhibited this kinetic dependence when H_2O was added to DME–O_2 reactants (Fig. 2). Thus, we conclude that OH* species were indeed the MASI species on Pd at all reaction conditions examined and became so on Pt at moderate H_2O pressures (>5 kPa). Equation (4) indicates that in both instances, the only rate constant relevant to the dynamics of combustion is k_2, reflecting the abstraction of H atoms from chemisorbed DME molecules. The other terms in the apparent rate constant reflect the thermodynamics of DME and H_2O chemisorption on Pd surfaces nearly covered with OH*, consistent with the isotopic studies reported next.

3.3. CH_3OCH_3–CD_3OCD_3 and H_2O–D_2O kinetic isotope effects

Kinetic isotope effects (KIE, r_H/r_D) were measured from combustion rates (at 1% DME conversion) with CH_3OCH_3 and CD_3OCD_3 reactants on 0.9 wt% Pd/ZrO_2 (0.17 dispersion; 2 kPa CH_3OCH_3 or CD_3OCD_3, 20 kPa O_2) at 473 and 503 K with added H_2O or D_2O (1 kPa). Measured KIE values are reported in Table 2. H/D exchange reactions on Pd clusters were not observed in any experiments (DME conversions, 0–42%); The amounts of CH_2DOCH_3, CHD_2OCH_3, and CD_3OCH_3 were below their respective mass spectrometric detection limits, indicating that the H/D exchange rates were $> \sim$200 times lower than the chemical conversion rates during reactions of CH_3OCH_3–O_2–D_2O mixtures at 473 K. The effect of deuterium on the rates from Eq. (4) is given by

$$\mathrm{KIE} = \frac{K_{1,\mathrm{H}} k_{2,\mathrm{H}} K_{3,\mathrm{H}}}{K_{1,\mathrm{D}} k_{2,\mathrm{D}} K_{3,\mathrm{D}}}. \tag{5}$$

Normal H–D isotope effects are expected for hydrogen abstraction steps (e.g., step 1.2, k_2); weaker thermodynamic isotope effects arise from quasi-equilibrated DME chemisorption steps and OH* recombination to form H_2O (step 1.1, K_1; step 1.3, K_3). Measured rates were higher for CH_3OCH_3–H_2O–O_2 than for CD_3OCD_3–H_2O–O_2 reactants (Table 2). These data are consistent with the kinetic relevance of C–H bond activation steps (step 1.2, k_2) in DME combustion. In contrast, CH_3OCH_3–H_2O and CH_3OCH_3–D_2O reactant mixtures gave similar turnover rates ($r_H/r_D = 1.0 \pm 0.05$), indicating that water activation (step 1.3) is not kinetically relevant and that inhibition effects reflect the quasi-equilibrium instead of the dynamics of this OH recombination; such thermodynamic effects give rise to weak isotope effects for the relevant equilibrium constant (K_3).

Previously, we reported KIE values for DME combustion on Pt-based catalysts (4.2 at 473 K and 3.2 at 503 K). We have considered two possible kinetically relevant steps, involving hydrogen abstraction from either undissociated adsorbed DME or from methoxides formed in irreversible activation of C–O bonds in adsorbed DME. These mechanistic choices were dictated by the lack of isotopic scrambling in isotopic mixtures of $^{18}O_2$–$^{16}O_2$ or $^{12}CH_3O^{12}CH_3$–$^{13}CH_3O^{13}CH_3$ reactants [8]. However, the measured KIE values and the kinetic response of DME combustion rates on DME and O_2 pressures are inconsistent with C–H activation in chemisorbed methoxides formed via irreversible DME dissociation on Pt surfaces [8]. Density functional theory estimates of the relative reactivity of C–H and C–O bonds in DME also have shown that C–H bond activation in chemisorbed DME molecules is much more favorable than the cleavage of its C–O bond to form chemisorbed methoxide species [8]. In the case of Pd, we again considered the possible formation and involvement of methoxide intermediates. A sequence of elementary steps involving irreversible DME dissociation (k_{diss}) and an H abstraction step from the resulting methoxides ($k_{\mathrm{H\text{-}abst}}$) is provided as an alternate step to H abstraction from molecularly adsorbed DME (step 1.2 in Scheme 1). These alternate steps give a simple rate equation for the case of OH* as MASI:

$$r = \frac{2K_1 K_3 k_{\mathrm{diss}}[\mathrm{DME}]}{[\mathrm{H_2O}]}. \tag{6}$$

The details of the derivation are given in Appendix A. This equation is also consistent with the kinetic data presented in Fig. 2 (Eq. (1)). We have found no other sequences or reversibility or MASI assumptions consistent with the measured rate data. But Eq. (6) does not contain rate constants for elementary steps involving C–H bond activation ($k_{\mathrm{H\text{-}abst.}}$), and it predicts weak thermodynamic isotope effects for DME chemisorption and OH* recombination (step 1.1, K_1; step 1.3, K_3) and for the kinetic parameter for irreversible DME dissociation (k_{diss}). These predictions are inconsistent with measured KIE values and rule out the involvement of chemisorbed methoxides as kinetically relevant intermediates in catalytic combustion of DME. Methoxide intermediates formed during CH_3OH oxidation on Pd clusters (42% dispersion) convert to CO_2 ($\sim$67% yield) at much lower temperatures (340 K) than those used in the present study for DME combustion [29]; therefore, any

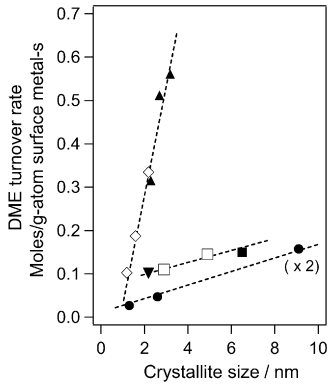

Fig. 4. DME combustion turnover rates as a function of metal dispersion on ZrO_2 and Al_2O_3 supports. (473 K, 2 kPa DME, 20 kPa O_2, 1% DME conversion, 5 mg Pt and Pd catalysts, 8 mg Rh catalyst, SiO_2: catalyst = 50:1; (◇) 0.9 wt% Pt/Al_2O_3, (▲) 1.0 wt% Pt/ZrO_2, (▼) 0.4 wt% Pd/Al_2O_3, (□) 0.7 wt% Pd/Al_2O_3, (■) 0.9 wt% Pd/ZrO_2, (●) 0.9 wt% Rh/Al_2O_3.)

methoxide groups formed after the first H-abstraction from molecularly adsorbed DME also would be immediately and irreversibly converted to CO_2 at 473 K with no intervening exchange reactions.

We conclude that measured kinetic isotope effects reported here on Pd catalysts also reflect, as in the case of Pt [8], combustion rates limited by H abstraction from methyl groups in molecularly adsorbed DME.

3.4. Effects of cluster size and metal identity on DME combustion turnover rates

Fig. 4 shows the effects of cluster size on DME combustion turnover rates on supported Pt, Rh, and Pd clusters. These crystallite size effects were previously described for Pt-based catalysts [8] and are reported here on Pd and Rh clusters [26–28] for the first time. Turnover rates shown in Fig. 4 were measured at the same low DME conversion levels (1%), to maintain similar average H_2O pressures on all catalyst beds without adding H_2O to DME–O_2 reactants. Rates on Pt were obtained by interpolating reactant and product average concentrations using Eq. (3) (O*: MASI), because kinetic dependences on Pt-based catalysts are consistent with those in Eq. (3) for conversions below ∼20% [8]. Rates on Pd were obtained by interpolating reactant and product average concentrations using Eq. (4), due to the kinetic inhibition prevalent at all DME conversions. Supported Rh clusters gave the lowest DME combustion turnover rates among these catalysts and formed trace amounts of CO and CH_3OH together with CO_2 and H_2O at these temperatures. On Rh, reaction rates in Fig. 4 were also interpolated using Eq. (4).

Two supports (Al_2O_3 and ZrO_2) were used to disperse Pt and Pd clusters. No support effects on turnover rates were detected for clusters with 0.2–0.9 dispersion. On Pt, Pd, and Rh clusters, DME turnover rates increased with increasing cluster size. Larger clusters expose low-index surfaces, whereas smaller metal clusters expose atoms with higher coordinative unsaturation, which are known to bind oxygen more strongly [30]. Smaller Pd and Rh clusters also reduce at higher temperatures and bind oxygen as metals more strongly than larger clusters in their metallic state [31–33], consistent with their greater affinity for oxygen atoms. Higher oxygen binding energies on small clusters make (O*)–(*) site pairs less favorable and thus decrease their density as well as that of chemisorbed DME intermediates involved in kinetically relevant H abstraction steps. They also decrease the basicity of the oxygen atoms relevant to H abstraction from adsorbed DME. These trends are consistent with the conclusion that DME combustion on Rh clusters proceeds via the elementary steps similar to those known to occur on Pt and Pd clusters (Scheme 1).

Table 3
Effective rate constants for DME combustion reaction

Catalyst	$K_1k_2K_3$[a] (mol/g atom surface metal s)
1.0 wt% Pt/ZrO_2 (0.42 dispersion)	0.82 ± 0.042
0.9 wt% Pd/ZrO_2 (0.17 dispersion)	0.03 ± 0.001

[a] Rate constants calculated by using Eq. (4) and measured DME turnover rates (Fig. 2a).

For a given cluster size, the identity of the metal influences surface reactivity and thus DME turnover rates. DME combustion involves redox cycles and vacancies on oxygen-covered Pt and Pd clusters (and on Rh clusters by inference from the similar cluster size effects but without direct mechanistic evidence). This leads to the observed zero-order dependence on O_2, the inhibition by water, and also the higher intrinsic reactivity of Pt, which has a lower intrinsic oxygen binding energy than Pd or Rh surfaces; for example, metal–oxygen bond energies calculated using density functional theory on (111) metal surfaces with 0.11 O* coverages increase in the sequence Rh (469 kJ mol^{-1}) > Pd (382 kJ mol^{-1}) > Pt (354 kJ mol^{-1}) [34].

The DME combustion rates shown in Fig. 4 reflect combinations of rate constants that differ between Pt [$4.5K_1^2k_2^2k_5^{-1}$; Eq. (3)] and Pd or Rh [$K_1k_2K_3$; Eq. (4)]. DME turnover rates on Pt clusters (0.42 dispersion: 2.7 nm) were ∼4 times higher than those on Pd clusters (0.17 dispersion: 6.5 nm) (Fig. 4). We note that combustion rates on Pt clusters at these conditions reflect the dynamics of the irreversible dissociative chemisorption step of O_2 (k_5) and the activation of C–H bonds in chemisorbed DME (k_2), but are unaffected by the relevant parameter for the quasi-equilibrated recombinative desorption of OH* species (K_3). As a result, the rates depend on DME and O_2 concentrations, but not on H_2O concentration, for the data in Fig. 4. In contrast, DME combustion rates on Pd reflect a different combination of rate and equilibrium constants [$K_1k_2K_3$; Eq. (4)] in the data shown in Fig. 4. Therefore, we compared Pt and Pd clusters in the presence of 5 kPa H_2O (Fig. 2a), because rates at these conditions reflect the value of the same combination of rate and equilibrium constants on these two catalysts [$K_1k_2K_3$; Eq. (4)]. Table 3 gives the apparent rate constants derived from regression of DME turnover rate data in Fig. 2a to the functional form of Eq. (4) on all catalysts. The relevant combination of rate constants on Pt clusters (0.42 dispersion: 2.7 nm) was ∼27 times higher than on Pd clusters (0.17 dispersion: 6.5 nm) (Table 3). This indicates that turnover rates on Pt clusters were indeed instrinsically higher than on Pd clusters, apparently because of the weaker binding energy of chemisorbed oxygen

atoms and hydroxyl groups on Pt clusters than on Pd, which in turn led to increases in the reactivity of O* for H abstraction (Scheme 1, step 1.2; k_2) and the availability of uncovered metal atoms (*) required for DME adsorption (Scheme 1, step 1.1; K_1 and step 1.3; K_3). Rate differences evident from the less-rigorous rate comparisons in Fig. 4 are much smaller (∼4-fold higher for Pt than for Pd). These latter comparisons cannot be rigorously interpreted in terms of the properties of each metal, because they reflect different combinations of kinetic and thermodynamic parameters on Pt ($4.5K_1^2k_2^2k_5^{-1}$) and on Pd ($K_1k_2K_3$).

We conclude that the effects of crystallite size, as well as those of metal identity, reflect the availability of (O*)–(*) site pairs during steady-state DME oxidation. This conclusion is consistent with the mechanistic proposal in Scheme 1 and with the measured kinetic dependences and isotope effects on supported Pt and Pd clusters. The kinetic response on Pd and Pt clusters (with H_2O in the latter case), and the effect of cluster size for DME combustion reaction resemble those reported for CH_4 combustion on Pd and Pt clusters [22,35]. Based on these observations and evidence, we conclude that these effects of size and metal identity and the rate equation measured for DME combustion rates represent general features of reactions requiring vacancies to stabilize intermediates on surfaces covered predominately by O* or OH* during catalysis and the involvement of basic oxygens in the activation of strong C–H bonds in kinetically relevant steps.

4. Conclusion

Kinetic and isotopic measurements provide a consistent mechanistic picture of DME combustion turnovers on Pd metal clusters. This reaction involves DME activation on site pairs consisting of an oxygen atom (O*) and a surface vacancy site (*), as also reported previously for Pt clusters. Reaction rates are limited by C–H bond activation in chemisorbed DME molecules to form methoxy methyl and hydroxyl surface intermediates on surfaces covered predominately by hydroxyl groups. The kinetic relevance of C–H bond activation on Pd clusters was confirmed by H/D kinetic isotope effect measurements. The rate equation derived from the proposed sequence of elementary steps is consistent with the kinetic response of DME turnover rates on Pd clusters to DME, O_2, and H_2O concentrations. The rate equation on Pd clusters resembled that on Pt clusters when H_2O was added in the latter case, and both surfaces were covered predominately by H_2O-derived OH groups. These similar kinetic responses suggest a mechanistic resemblance, but with stronger H_2O inhibition effects in the case of Pd clusters. The addition of H_2O was required to cover Pt surfaces with OH*, whereas H_2O products (even at low DME conversions) led to near-saturation of Pd surfaces with OH* under all reaction conditions. DME turnover rates increased with increasing crystallite size in the order Pt > Pd > Rh for a given cluster size. These effects of crystallite size and metal identity reflect the availability of (O*)–(*) site pairs required for kinetically relevant H abstraction steps from DME adsorbates during steady-state DME combustion turnovers.

Acknowledgments

This study was supported by BP as part of the Methane Conversion Cooperative Research Program at the University of California Berkeley. The authors thank Drs. Aditya Bhan and Nan Yao, Ms. Cathy Chin, and Mr. Brian Weiss, University of California Berkeley for helpful technical discussions and their comments on the manuscript.

Appendix A. Derivation for the kinetic equations described in Section 3.3 (Assumption: methoxide formation)

The pseudo-steady-state approximation is used to solve for $[CH_3O^*]$ and $[O^*]$,

$$\frac{d[CH_3O^*]}{dt} = 2k_{diss}[CH_3OCH_{3-*}][O^*] - k_{H\text{-}abst}[CH_3O^*][O^*] = 0 \quad (A.1)$$

and

$$\frac{d[O^*]}{dt} = 2k_5[O_2][^*]^2 - 4k_{H\text{-}abst}[CH_3O^*][O^*] - k_{diss}[CH_3OCH_{3-*}][O^*]. \quad (A.2)$$

$[CH_3OCH_{3-*}]$ and $[CO_2^*]$ are solved using quasi-equilibrium approximations in terms of (*),

$$[CH_3OCH_{3-*}] = K_1[CH_3OCH_3][^*] \quad (A.3)$$

and

$$[CO_2^*] = \frac{[CO_2][^*]}{K_4}. \quad (A.4)$$

Therefore, Eqs. (A.1) and (A.2) become

$$[CH_3O^*] = \frac{2k_{diss}[CH_3OCH_{3-*}]}{k_{H\text{-}abst}} = \frac{2K_1k_{diss}[CH_3OCH_3][^*]}{k_{H\text{-}abst}} \quad (A.5)$$

and

$$[O^*] = \frac{k_5[O_2][^*]}{4.5K_1k_{diss}[CH_3OCH_3]}. \quad (A.6)$$

The concentration of [OH*] is solved using quasi-equilibrium approximations in terms of (*), after which it becomes

$$[OH^*] = \left(\frac{k_5[H_2O][O_2]}{4.5K_1K_3k_{diss}[CH_3OCH_3]}\right) \times [^*], \quad (A.7)$$

where C_t is the sum of the concentration of the species on PdO_x surface,

$$C_t = [^*] + [O^*] + [CH_3OCH_{3-*}] + [CH_3O^*] + [OH^*] + [CO_2^*]. \quad (A.8)$$

The rate of DME combustion is

$$r = k_{H\text{-}abst}[CH_3O^*][O^*], \quad (A.9)$$

$$r = \frac{2k_5[O_2]}{4.5 \times \left(1 + \left(\frac{k_5[O_2]}{4.5K_1k_{diss}[CH_3OCH_3]}\right) + K_1[CH_3OCH_3] + \frac{2K_1k_{diss}[CH_3OCH_3]}{k_{H\text{-}abst}} + \left(\frac{k_5[H_2O][O_2]}{4.5K_1K_3k_{diss}[CH_3OCH_3]}\right)^{0.5} + \frac{[CO_2]}{K_4}\right)^2}$$

$$* \quad O^* \quad DME^* \quad CH_3O^* \quad OH^* \quad CO_2^*$$

Equation A.10.

which, after substitution, becomes Eq. (A.10). When OH* becomes MASI, Eq. (A.10) becomes Eq. (6):

$$r = \frac{2K_1K_3k_{diss}[DME]}{[H_2O]}.$$

References

[1] T.H. Fleisch, A. Basu, M.J. Gradassi, J.G. Masin, Stud. Surf. Sci. Catal. 107 (1997) 117.
[2] J.-L. Li, X.-G. Zhang, T. Inui, Appl. Catal. A Gen. 147 (1996) 23.
[3] H.J. Curran, S.L. Fisher, F.L. Dryer, Int. J. Chem. Kinet. 32 (2000) 741.
[4] S.M. Japar, T.J. Wallington, J.F.O. Richert, J.C. Ball, Int. J. Chem. Kinet. 22 (1990) 1257.
[5] M.E. Jenkin, G.D. Hayman, T.J. Wallington, M.D. Hurley, J.C. Ball, O.J. Nislesen, T. Ellermann, J. Phys. Chem. 97 (1993) 11712.
[6] H.J. Curran, W.J. Pitz, C.K. Westbrook, P. Dagaut, J.-C. Boettner, M. Cathonnet, Int. J. Chem. Kinet. 30 (1997) 229.
[7] S.L. Fisher, F.L. Dryer, H.J. Curran, Int. J. Chem. Kinet. 32 (2000) 713.
[8] A. Ishikawa, M. Neurock, E. Iglesia, J. Am. Chem. Soc. (2007), doi: 10.1021/ja073712z.
[9] R.A. Dalla Betta, Catal. Today 35 (1997) 129.
[10] J.K. Lampert, M.S. Kazi, R.J. Farrauto, Appl. Catal. B Environ. 14 (1997) 211.
[11] A. Ishikawa, E. Iglesia, Chem. Commun. (2007) 2992.
[12] A. Yamaguchi, E. Iglesia, unpublished results.
[13] J. Wei, E. Iglesia, J. Phys. Chem. B 108 (2004) 4094.
[14] R. Burch, F.J. Urbano, Appl. Catal. A Gen. 124 (1995) 121.
[15] D. Ciuparu, E. Altman, L. Pfefferle, J. Catal. 203 (2001) 64.
[16] J.H. Lee, D.L. Trimm, Fuel Process. Technol. 42 (1995) 339.
[17] P. Papaefthirniou, T. Ioannides, X.E. Verykios, Appl. Catal. B Environ. 13 (1997) 175.
[18] J. Wei, E. Iglesia, J. Phys. Chem. B 108 (2004) 7253.
[19] R.L. David, Handbook of Chemistry and Physics, 87th ed., CRC Press, Boca Raton, FL, 2006, pp. 4.43–4.101.
[20] G.L. Kellogg, Surf. Sci. 171 (1986) 359.
[21] G. Ketteler, D.F. Ogletree, H. Bluhm, H. Liu, E.L.D. Hebenstreit, M. Salmeron, J. Am. Chem. Soc. 127 (2005) 18269.
[22] K. Fujimoto, F.H. Ribeiro, M. Avalos-Borja, E. Iglesia, J. Catal. 179 (1998) 431.
[23] R.W. Joyner, J. Chem. Soc. Faraday Trans. I 76 (1980) 357.
[24] C.B. Wang, H.K. Lin, S.N. Hsu, T.H. Huang, H.C. Chiu, J. Mol. Catal. A Chem. 188 (2002) 201.
[25] N. Seriani, W. Pompe, L.C. Ciacchi, J. Phys. Chem. B 110 (2006) 14860.
[26] C.T. Williams, C.G. Takoudis, M.J. Weaver, J. Catal. 170 (1997) 207.
[27] H.Y.H. Chan, C.T. Williams, M.J. Weaver, C.G. Takoudis, J. Catal. 174 (1998) 191.
[28] C.T. Williams, C.G. Takoudis, M.J. Weaver, J. Phys. Chem. B 102 (1998) 406.
[29] R.W. McCabe, P.J. Mitchell, J. Catal. 103 (1987) 419.
[30] Y. Xu, W.A. Shelton, W.F. Schneider, J. Phys. Chem. B 110 (2006) 16591.
[31] K. Otto, L.P. Haack, J.E. de Vries, Appl. Catal. B Environ. 1 (1992) 1.
[32] C.P. Hwang, C.T. Yeh, Q. Zhu, Catal. Today 51 (1999) 93.
[33] C.B. Wang, C.T. Yeh, J. Mol. Catal. A Chem. 120 (1997) 179.
[34] R.A. van Santen, M. Neurock, Molecular Heterogeneous Catalysis, Wiley–VCH, Weinheim, 2006, p. 107.
[35] M. Li, Y.H. Chin, J. Wei, E. Iglesia, unpublished results.